

Gold nanoparticles: assembly and electrical properties in 1–3 dimensions

G. Schmid*^a and U. Simon^b

Received (in Cambridge, UK) 30th July 2004, Accepted 20th October 2004

First published as an Advance Article on the web 16th December 2004

DOI: 10.1039/b411696h

Ligand stabilized gold nanoparticles have attracted much attention in the search for new chemically designed compounds for a future information technology, based on single-electron devices. This article gives an overview about the strategies used to synthesize and to assemble uniform gold nanoparticles in different dimensions as well as about the present status of the electrical properties of these. Examples are given for three-dimensional organisations, for the formation of self-assembled monolayers as well as for one-dimensional assemblies.

Introduction

According to the present paradigm of electronic information storage and exchange, continuous miniaturization of micro-electronic devices turns out to be the only evident concept for improving the performance of integrated circuits. There is some common belief in semiconductor industries that complementary metal oxide semiconductor (CMOS) scaling will continue for the next 10–15 years to reach its functional limits. At least at that point new concepts for scalable technologies need to be developed, and therefore the search for the most promising materials, processes and structures have inspired a lot of academic and industrial working groups to synthesize and to exploit the electrical transport properties of nanomaterials and molecular assemblies for the design of functional systems on the nanometre level.

One of the most promising concepts is the development of single-electron devices which retain their scalability down to the molecular level. At present, due to exploitation of charging

effects or so-called Coulomb effects in metallic single-electron devices comprising tunnel junctions with sub-micrometre size, individual charge carriers can be handled. This field was named Single Electronics (SE).¹ Although charging effects have earlier been observed in granular thin metal films,² SE as a direction in its own right was born more in the late 1980s, when ultra-small metal–insulator–metal (MIM) sandwich structures (tunnel junctions) and simple systems of these have started to be intensively studied both theoretically and experimentally.³ The discreteness of the electric charge becomes essential and the tunneling of electrons in a system of such junctions can be affected by the Coulomb interaction of electrons which can be varied by an externally applied voltage or by injected charges. The simplest arrangement for a two-terminal device is a metal island between two metallic electrodes separated from each other by a dielectric environment. By transferring a single electron from the electrodes to the island by applying a certain voltage, the island is charged negatively and the electrodes keep the positive image charge, whereas the overall charge is kept to zero. In this situation, the electrostatic energy, *i.e.* the single electron charging energy $E_c = e^2/2C$ where e is the elementary charge and C is the self-capacitance of the metallic island, is stored in the arrangement. If $E_c \gg k_B T$, thermal fluctuation of the charge is suppressed and the threshold voltage has to overcome the Coulomb blockade to add an electron *via* the source electrode or to let it leave *via* the drain electrode. If, for instance, the diameter of the metal island is about 1 μm and the dielectric constant of the environment is $\epsilon = 5$, E_c exceeds $k_B T$ at about $T = 4$ K. Consequently, by decreasing the island size down to 1–2 nm, single electron movements can be controlled even in the range of room temperature.

Different approaches have been discussed up to now on how to bridge the size gap between the conventionally fabricated circuit elements (*e.g.* CMOS) of some 10 nm in size and at least the true atomic scale in the future. In that concern gold nanoparticles have attracted much attention. They can be synthesized with a distinct particle size of 2 nm or less, and the large charging energy, which is determined by the particle size and their embedding into the respective “environment”, *i.e.* a ligand shell or linking molecules, means they fulfil the prerequisites to be used as central elements in single electron devices at room temperature and above. This has been shown

*guenter.schmid@uni-essen.de

Günter Schmid was born in Villingen, Germany in 1937 and studied chemistry at the University of Munich. He received his diploma in 1962 and his doctoral degree in Inorganic Chemistry in 1965, both at the University of Munich. In 1966 he moved to the University of Marburg, Germany, and finished his habilitation in 1969. In 1971 he got a professorship at the University of Marburg and then he moved to the University of Essen, Germany, where he became the director of the Institute for Inorganic Chemistry (1977). His main research interests include the synthesis and investigation of large transition metal clusters and colloids, the generation of three-, two- and one-dimensional arrangements of quantum dots, heterogeneous catalysis, and nanotechnology.

Ulrich Simon was born in Essen in 1963. He studied chemistry at the University of Essen and obtained his diploma in 1990. In 1992 he obtained his doctorate (Dr. rer. nat.) in Essen and his habilitation in 1999. Since May 2000 he has held the chair of Inorganic Chemistry and Electrochemistry at the Aachen University of Technology (RWTH). The main interest of his current research includes the synthesis, the characterization and the electrical properties of nanostructured materials.

repeatedly in many works using different experimental techniques. Most results have been obtained from scanning tunneling spectroscopy and in recent years the fabrication of nanoelectrode devices has made a great impact on this field of research. Nevertheless, the use of these chemically tailored nanomaterials for device fabrication requires parallelized and scalable methods for self assembly into functional units in one, two or three dimensions. Furthermore, one needs to find out and to understand the many control parameters for a directed assembly and for the adjustment of the electrical transport properties to the desired application. This will be undoubtedly one of the greatest challenges in the materials chemistry of nanoparticles.

With this article we intend to acquaint the reader with the methods of synthesis of ligand stabilized gold nanoparticles, their assembly in three, two and one dimension(s) and with the electrical properties of these.

Three-dimensional arrangements

Three-dimensional (3D) organization means in principle nothing but crystallisation. Crystallisation happens usually between identical molecules and particles or between oppositely charged ions. However, as it turned out, 3D architectures can also be built up of colloidal particles (nanoparticles) the sizes and shapes of which are not fully identical. Of course, a rather small size distribution of nanoparticles is a condition to get crystals. The 3D organization of nanoparticles can also be reached by the use of spacers, linking the particles. Due to their special electronic behaviour, the ligand stabilized Au_{55} clusters are the focus of interest with respect to organization processes in all dimensions. Another reason is their monodispersity, making organization processes less complicated. $\text{Au}_{55}(\text{PPh}_3)_{12}\text{Cl}_6$ is the most easily available representative of this cluster family. Numerous derivatives with other ligands have become known and can be generated by ligand exchange reactions.⁴

$\text{Au}_{55}(\text{PPh}_3)_{12}\text{Cl}_6$ crystallizes spontaneously from dichloromethane solution if the solvent is evaporated. However, this process only results in small micrometre-sized single crystals. The time consuming formation of larger crystals fails due to continuous decomposition in solution. Fig. 1 shows a transmission electron microscope (TEM) image of some of those microcrystals, prepared on the TEM grid from solution.⁵

There exist two other versions of Au_{55} nanoclusters that have been prepared by very special procedures. If a small volume of a dichloromethane solution of $\text{Au}_{55}(\text{PPh}_3)_{12}\text{Cl}_6$ clusters is kept under water until the organic solvent has been removed by diffusion, micrometre-sized crystals remain which are, isolated and dried, no longer soluble in dichloromethane, indicating that there must be a change in the chemical composition. Probably due to the intensive contact between water and the dichloromethane solution hydrolysis of the chlorine atoms happens.⁶ XPS investigations of the crystals clearly show the absence of chlorine, in contrast to the original material where a signal at ~ 269 eV indicates the presence of Cl (Cl-2s). The lack of a Cl signal also excludes involvement of CH_2Cl_2 in the crystallisation process. Electron diffraction of the crystals shows bcc packed structures, whereas the starting

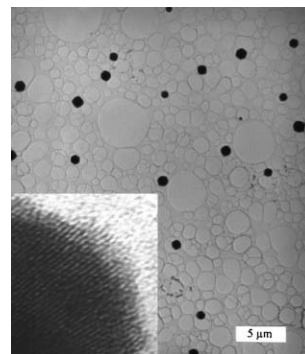


Fig. 1 Transmission electron microscope (TEM) image of typical microcrystals of $\text{Au}_{55}(\text{PPh}_3)_{12}\text{Cl}_6$, formed on the grid from CH_2Cl_2 solution.

compound crystallizes fcc.⁵ In Fig. 2 a scanning electron microscope (SEM) image of such microcrystals is presented.

It is not yet clear how the Au_{55} clusters are linked together in these crystals. XPS not only shows the absence of chlorine, but also the presence of phosphine coordinated gold (XPS signal at 189 eV, P-2s). In any case the crystals imaged in Fig. 2 still consist of Au_{55} nuclei as building blocks coordinated by PPh_3 , but not by Cl atoms. The existence of Au–O–Au-bridges would be rather unusual, but cannot be excluded completely since water is the only component.

The quantitative removal of the ligands in $\text{Au}_{55}(\text{PPh}_3)_{12}\text{Cl}_6$ is possible too, however, under very unusual conditions. If the cluster compound is reacted with an excess of the 4th generation dendrimer G4-SH, equipped with 96 terminal SH functions, all phosphines and, as far as can be seen, also the chlorines are eliminated to grow to $(\text{Au}_{55})_n$ superstructures, again appearing as perfect micrometre-sized crystals. One of them is shown in Fig. 3 as a TEM image.⁷

The process resulting in this surprising product is believed to consist of the formal substitution of the phosphine ligands by the stronger SH groups of the dendrimers, however, the mobility of the particles on the dendrimers' surfaces enables strong Au–Au contacts, finally ending up in crystal growth inside a sphere of dendrimers.

As can be seen from these results, the uniform Au_{55} nanoparticles strongly tend to form 3D crystals with, as well as without ligands. Bare Au_{55} clusters are very stable due to their ideal cuboctahedral structure, representing a member of the so-called full-shell clusters. As has been shown, these

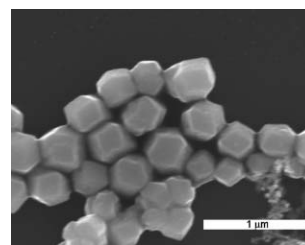


Fig. 2 Scanning electron microscope (SEM) images of microcrystals of bcc-structured Au_{55} clusters, prepared by contact of CH_2Cl_2 solutions with water.

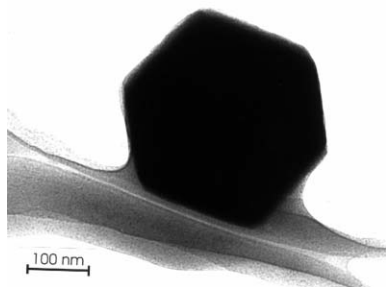


Fig. 3 TEM image of a microcrystal consisting of perfectly ordered bare Au₅₅ clusters.

clusters cannot be oxidized in an oxygen plasma, whereas numerous smaller and larger gold nanoparticles, even the surfaces of bulk gold could be oxidized under the same conditions.⁸

For the study of charge transport between Au₅₅ nuclei it is important to vary the distance between them. This can be done by changing the kind of ligands on the cluster's surface or by linking them *via* spacer molecules. For variations of the ligand shell, except PPh₃, bulkier molecules such as silsesquioxanes can be used, doubling the cluster–cluster distance from 2.2 nm.⁹ Fig. 4 shows models of both types.

The sulfonated ligand molecule Ph₂PC₆H₄SO₃H can be used to interconnect clusters by diamines *via* ionic attractions (type II in Fig. 5).¹⁰

In contrast to such cluster combinations, those based on covalent interconnections can be prepared by using dithiols. Thiols easily substitute phosphines and so form strong Au–S bonds. Fig. 5 elucidates the situation between the different kinds of cluster–cluster interactions. The non-covalently and the covalently connected clusters in 3D assemblies should characteristically differ in charge transport properties between them; this will be shown in the following by measuring the activation energies from ac and dc measurements.¹⁰

The electrical behavior of these three-dimensional systems has intensively been studied by dc and ac (complex impedance) measurements.^{11,12} As a common feature, at high temperature,

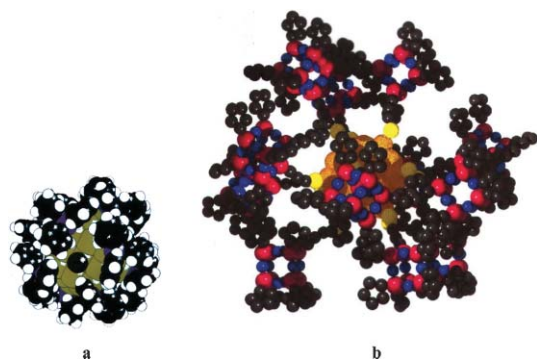


Fig. 4 Models of Au₅₅ clusters, protected by two different types of ligands: PPh₃ (a) resulting in a diameter of *ca.* 2.2 nm, and (cyclopentyl)₇Si₈O₁₂(CH₂)₃SH (b), enlarging the diameter to *ca.* 4.2 nm.

i.e. several tens of Kelvin below room temperature, the temperature dependence of the dc and of the ac conductivity shows a simply activated behavior according to the Arrhenius relation:

$$\sigma(T) = \sigma_0 + \exp\left(\frac{-E_A}{k_B T}\right)$$

where E_A is the activation energy, and $k_B T$ is the characteristic thermal energy. This reflects classical hopping transport of individual charges between nearest neighboring particles (nearest neighbor hopping). E_A becomes temperature dependent when the measuring temperature is decreased. This means that down to very low temperatures the conductivity follows the variable range hopping (VRH) expression, proposed by Mott:¹³

$$\sigma(T) = \sigma_0 + \exp\left(\frac{-T_0}{T}\right)^\gamma$$

where $\gamma = 1/(D + 1)$ in D dimensions. Although $\gamma = 1/4$ ($D = 3$) might be expected from this general expression, $\gamma = 1/2$ ($D = 1$) is predominantly observed in the case of the compacted metal cluster compounds. This temperature dependence, as well as the electric field dependent conductivity which reflects pronounced non-ohmic behavior at strong electric fields, discloses a pronounced similarity to different heterogeneous materials, like cermets, doped and amorphous semiconductors, or metal– and carbon–insulator composites. This behavior was carefully analyzed by applying different physical models of hopping conductivity with the conclusion that at low temperatures the experimental data can be approached with a thermally activated stochastic multiple site hopping process, whereas at high temperatures around room temperature nearest neighbor hopping dominates.^{14–16}

This means that at low temperature the number of charge carriers participating in the hopping process does not change with temperature. Instead, at high temperatures, where $k_B T$ becomes comparable to the charging energy E_c of the metal particle (note that E_c is determined by the total capacitance of the particle, and is therefore dependent on the particle size as well as on the inter-particle spacing, *i.e.* the dot-to-dot distance), thermally excited extra charge carriers are participating in the hopping process. Thus, even at high temperature, the activation energy reflects the energy needed to transfer one electron from an electrically neutral particle to another. Chemically speaking, this is the charge disproportionation energy and it has its atomic analogue in the disproportionation energy of atoms, ions or molecules in chemical redox-reactions.

Quantized capacitance charging, also reflecting such a multivalent redox-like behavior, has also been observed in cyclic voltammetric measurements, where monolayers of nanoparticles were used as electrodes.^{17,18} For small particles with 140 atoms or less, even molecule-like behavior reflecting a size dependent HOMO–LUMO gap is observed.¹⁹

Since at high temperature (around room temperature) nearest-neighbor hopping is dominant, it has become an interesting question whether the charging energy of such cluster materials can chemically be tailored by means of bifunctional spacer molecules, which define the inter-particle spacing by the molecule length. This concept has been realized with the family of ligand stabilized Au₅₅ clusters by ligand

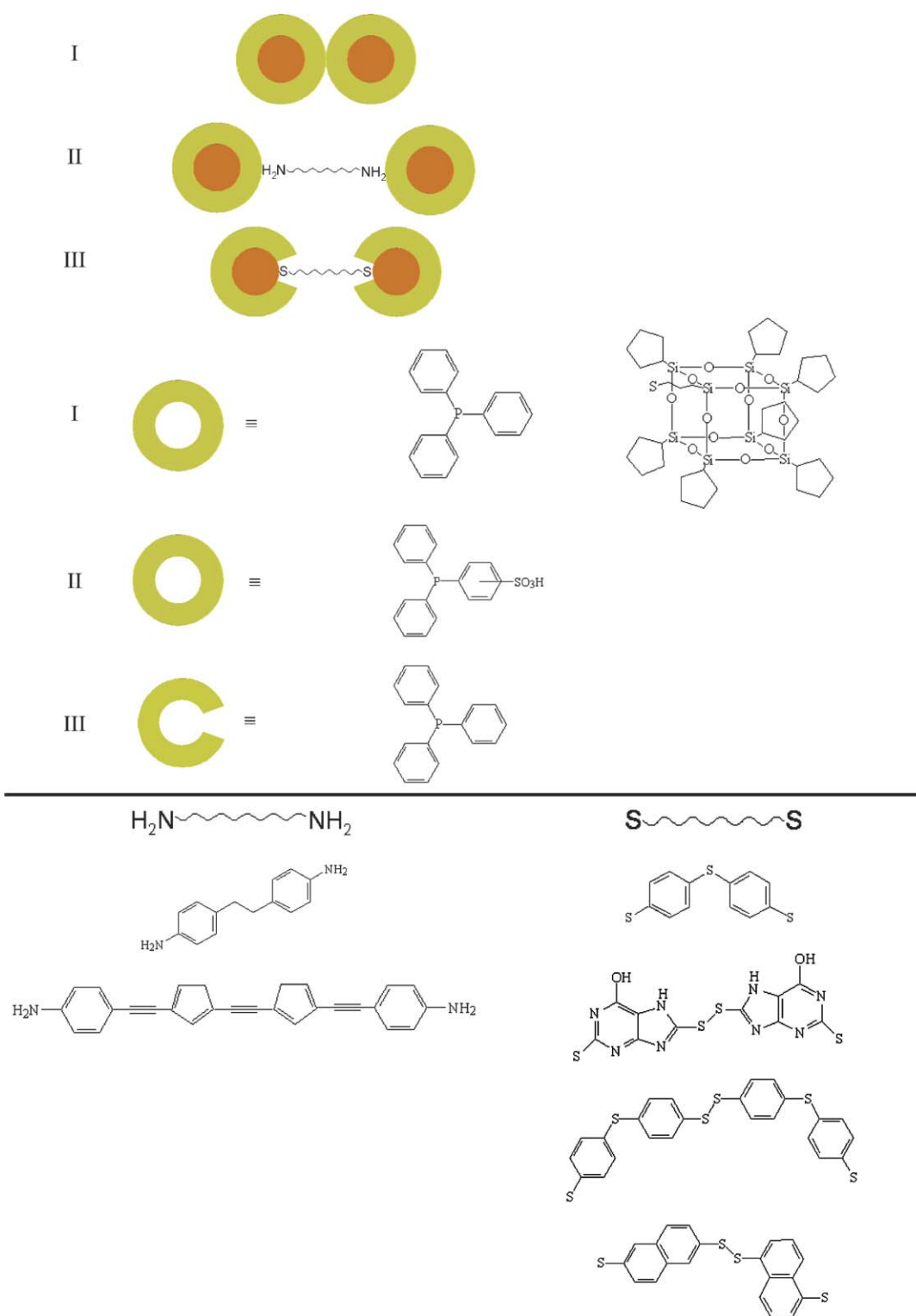
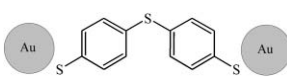
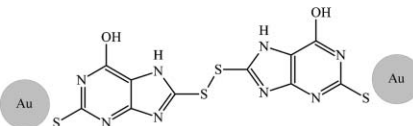
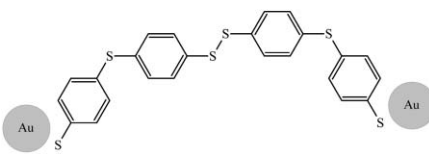
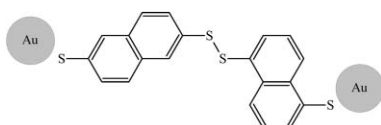
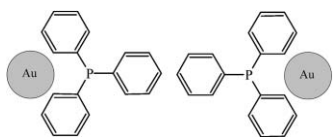
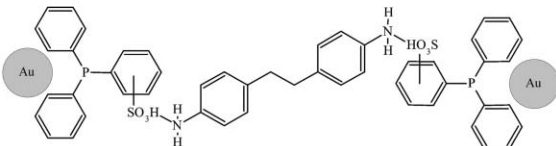
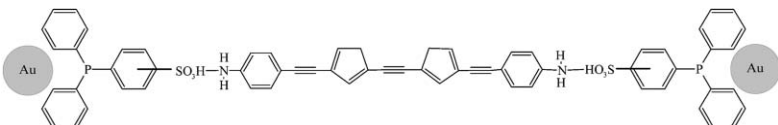
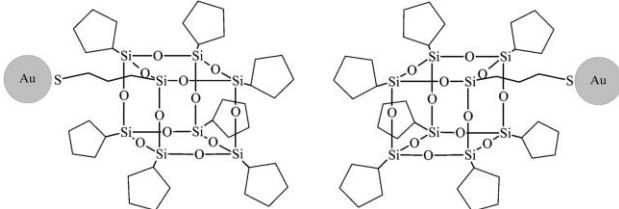


Fig. 5 Various types of cluster-cluster interactions.

exchange reaction, as described before.¹¹ While the cluster size is kept constant when the cluster spacing is increased by the spacer molecules, an almost linear increase of the activation energy is observed. This can be explained by a decrease of the junction capacitance C , which scales with $1/d$ (d = particle spacing) as long as the other geometric and dielectric

parameters are kept constant. This relation is valid as long as the spacer molecules are not covalently bound to the cluster surface and the spacer molecules have no delocalized π -electron system along their backbone between its termini. As soon as covalently linking species equipped with delocalized π -electrons enable inter-cluster electron

Table 1 Activation energies and cluster-cluster distances of covalently and non-covalently organized systems

Covalently linked			
Linking system	Distance/nm	E_a/eV	
	1	1.1	0.095
	2	1.6	0.11
	3	2.3	0.12
	4	1.5	0.14
Non-covalently linked			
Linking system	Distance/nm	E_a/eV	
	5	0.7	1.6
	6	1.9	2.0
	7	2.8	2.3
	8	3.1	2.6

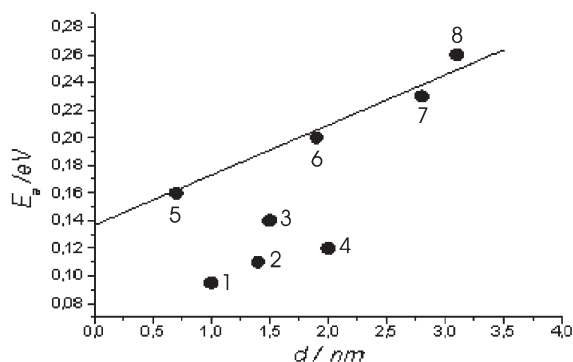


Fig. 6 Activation energies versus cluster–cluster distances of the covalently (1–4) and the non-covalently (5–8) organized systems (Table 1).

transfer, the respective activation energy drops, dependent on the electronic structure of the molecules and their respective lengths.

These results are illustrated in Fig. 6, representing the activation energies versus cluster–cluster distance of the covalently and non-covalently linked cluster materials as summarized in Table 1.

While the activation energy increases continuously for the non-covalently linked cluster systems, the covalently bound, conjugated π -systems let the activation energy drop down to significantly lower values. These experimental findings can be compared with the mechanisms of classical redox processes in molecular complexes which have been divided into “outer-sphere” and “inner-sphere” charge transfer mechanisms.^{20,21} According to this model, the inner-sphere transfer of electrons is associated with the participation of a bridging ligand between the oxidizing and the reducing metal center, respectively. The outer-sphere electron transfer appears between coordinated metal centers, which simply touch each other *via* their coordination spheres. In this situation the electron transfer has to occur through the ligand shell and probably involves the deformation of the coordination spheres. Thermally activated electron transfer between metal clusters can apparently be compared with this classical model, since the initial step for the creation of free charge carriers is the charge disproportionation between initially neutral nanoparticles, representing the oxidation and the redox reaction, respectively. This leads to the assumption that, depending on the model to describe the charge transport mechanism, either the effective barrier height is reduced, or the transmission probability for electron tunneling through the barrier is increased when a spacer with a delocalized π -backbone is covalently bound to the cluster.

To distinguish between a temperature independent tunneling term and the thermally activated over-barrier process, a precise knowledge of the cell constant (*i.e.* the geometry parameters of the sample) is needed, as described by Wuelfing *et al.*²² However, this approach is not applicable to the experiments described here, since they do not provide the full information needed to take into account the sample geometry, the degree of disorder as well as the distribution of particle size and of the electrical field.

Thin films and monolayers

Although the 3D systems are structurally and electrically well characterized, with respect to future applications the nanoparticles have to be organized in 2 and in 1 dimensions. Here, one needs to take into account that not only the control over the deposition rate and density, but also the degree of order or disorder, respectively, which is vital for any kind of further technological developments. Thus, the generation of multilayers or even better of monolayers is a worthwhile challenge to perform the necessary electric investigations. There have been several approaches successfully performed during recent years which will be presented by means of selected examples.

One principle how to make—in general—non-ordered mono- and multilayers of ligand stabilized Au_{55} clusters is illustrated in Fig. 7. A self-assembled monolayer of appropriate thiol molecules on a flat substrate attracts the clusters from solution due to the already mentioned easy substitution of phosphines by thiols. A second, third, *etc.* layer can then be added by generating a second, third, *etc.* monolayer of dithiol molecules. This approach works quite satisfyingly. The layered structures can be observed by TEM images of sliced samples.²³

Densely packed but non-ordered monolayers of $\text{Au}_{55}(\text{PPh}_3)_{12}\text{Cl}_6$ can also be gained when oxidized GaAs wafer surfaces are first covered by a self-assembled monolayer of 3-mercaptopropyl-trimethoxysilane, followed by deposition of the clusters from solution. Fig. 8 shows an AFM image of an as-prepared monolayer. From the cross-section the almost perfect agreement of the layer thickness with the calculated value can be concluded. A similar result is obtained if a clean GaAs surface is decorated with a self-assembled monolayer of 1,4-dithiobenzene, followed by cluster deposition from solution.²⁴ Fig. 8 shows the AFM result, again in complete agreement with the calculated height.

Several approaches to measure the $I(U)$ behavior of $\text{Au}_{55}(\text{PPh}_3)_{12}\text{Cl}_6$ monolayers failed up to now, due to a too low overall conductivity. This is due to the fact that, on the one hand, $\text{Au}_{55}(\text{PPh}_3)_{12}\text{Cl}_6$ has a large charging energy making the whole system very sensitive towards structural disorder. On the other hand, it is extraordinarily difficult to control the cluster–electrode connection, *i.e.* the interface between the nanoparticles and the micro- or even nanostructured electrodes. In contrast, conductivity measurements of multilayers as

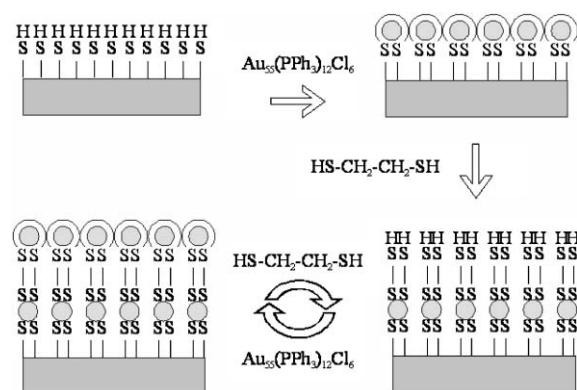


Fig. 7 Sketch of the layer-by-layer formation with linking dithiols.

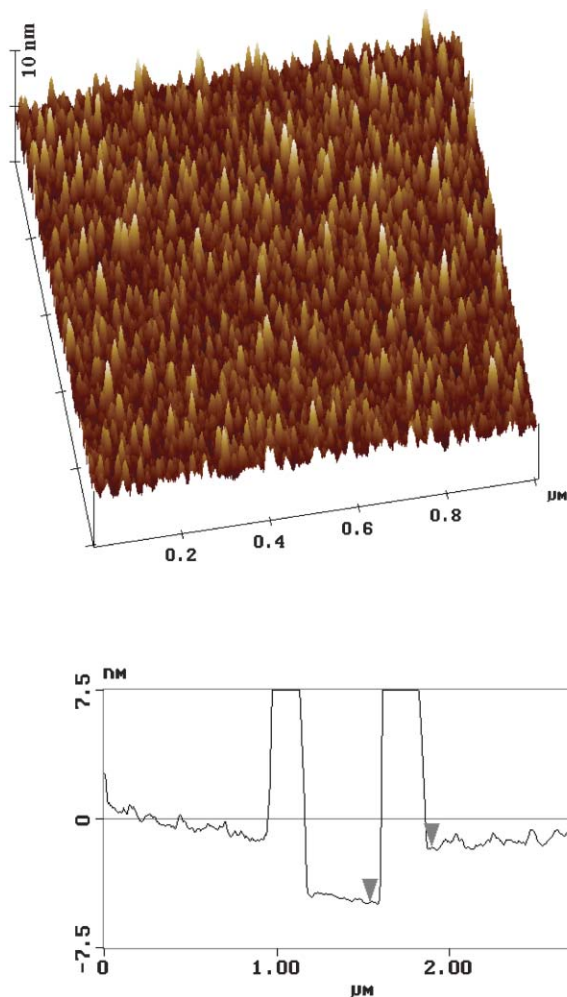
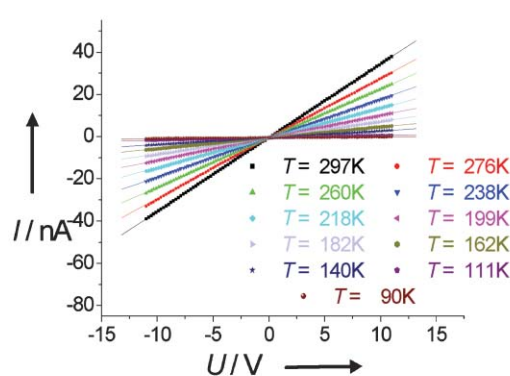


Fig. 8 AFM image of a 1,4-benzenedithiol modified GaAs surface covered with Au₅₅ clusters together with the height profile.

described above and of monolayers consisting of larger gold nanoparticles succeeded.

The electrical response of multilayers is very similar to those of the 3D systems. $I(U)$ and impedance measurements on multilayers of Au₅₅ show an almost linear response but a distinctly higher resistance as compared to the 3D samples.



The thermally activated conductivity shows again a transition from simply activated conductivity to a variable range hopping process at lower temperature. According to Mott's conductivity law, the charge transport should appear in quasi-one-dimensional current paths, since the temperature dependent conductivity could best be fitted with $\gamma = 1/2$ ($D = 1$) (see Fig. 9).

In contrast, monolayers of 15 nm gold particles show a non-linear $I(U)$ curve (see Fig. 11), but simply activated behaviour over a large temperature range, while a compact 3D solid of these nanoparticles shows metallic behaviour.²⁵ The layers have been assembled on a silicon substrate, which was modified with 3-aminopropyltrimethoxysilane (APTS). On this layer the citrate stabilized gold particles, synthesized according to a well established protocol, were deposited from an aqueous solution (pH 5). Since the solution of the nanoparticles was slightly acidic, adding this solution to the amino-silylated substrates led to the protonation of the amino groups on the surface. Such positively charged substrate surfaces enabled electrostatic attraction of negatively charged citrate stabilized gold nanoparticles. AFM-measurements showed a densely-packed monolayer of gold colloids with an average density of about 1500 particles per μm^2 as can be seen in Fig. 10.

In the case of these large particles, the activation energy, reflecting the charging energy of the nanoparticles, is

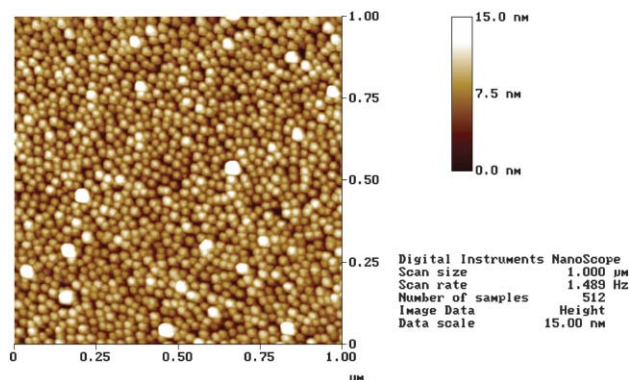


Fig. 10 AFM image of a 15 nm citrate stabilized gold particle monolayer, immobilized due to electrostatic attraction.

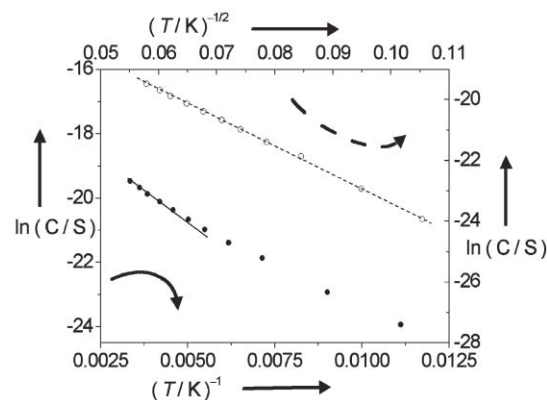


Fig. 9 Temperature-dependent $I(U)$ curves (a) and Arrhenius ($1/T$) and Mott ($1/\sqrt{T}$) plots for five layers.

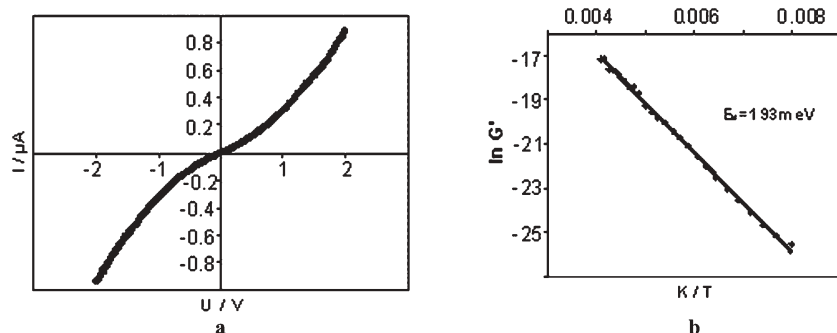


Fig. 11 $I(U)$ curve of a gold nanoparticle monolayer at room temperature (a) and an Arrhenius plot (b) of a 15 nm Au particle layer, attained by electrostatic immobilization.

predominately determined by the inter-particle spacing and not by the size of the individual particles. In this example the average spacing is adjusted by the thickness of the citrate shell including its ion cloud (center-to-center distance 6.8–7.2 nm), resulting in electrostatic control of the maximum density, which can be achieved by this method. The electrical field dependence of the conductivity reflects the behaviour of a 2D percolation network, but it may also result from the electrostatic charge the particles are wearing. This may lead to reorientational movement of the particles under the influence of strong electric fields.

Well ordered monolayers of $\text{Au}_{55}(\text{PPh}_3)_{12}\text{Cl}_6$ clusters become available if they are deposited on thin films of appropriate polymers such as poly(ethyleneimine) (PEI), poly(phenylenealkynyls) (PPE) or poly(vinylpyrrolidone) (PVP).²⁶ One example how those monolayers can be performed is schematically shown in Fig. 12.

A liquid two-phase system, consisting of water and dichloromethane (top!) is used to first generate a thin film of a suited polymer at the phase boundary. Addition of a few clusters to the top dichloromethane layer leads to fast deposition of the clusters on the polymer in a well ordered manner. The success of this ordering process is due to weak interactions between the polymer film and the ligand shell of

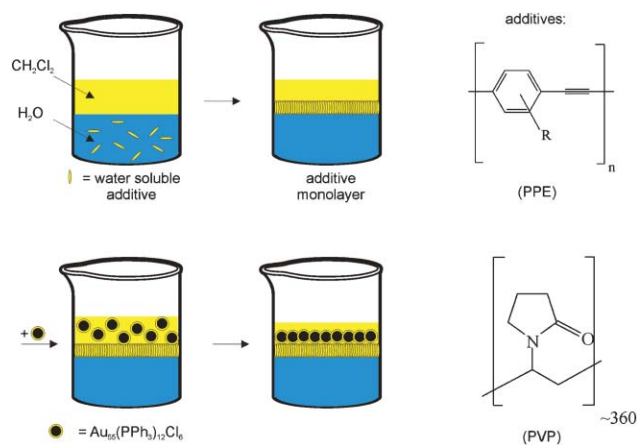


Fig. 12 Generation of ordered monolayers of $\text{Au}_{55}(\text{PPh}_3)_{12}\text{Cl}_6$ at the phase boundary of water/dichloromethane, supported by thin polymer films.

the gold clusters. The forces must be strong enough to attract the nanoparticles from solution, but weak enough to let them move around to get organized. Poly(methylmethacrylate) (PMMA), for instance, does not work.

Two kinds of structures could be observed: a hexagonal close-packed one and a primitive square one. Which one of the two is formed cannot be foreseen. It can be assumed that it depends accidentally on the very first contacts between a few cluster molecules and the orientation of the triphenylphosphine ligands to each other, as is indicated in Fig. 13.²⁷ Fig. 14 shows TEM images of cutouts of square-structured monolayers with increasing magnification.²⁸

Approaches to one-dimensional arrangements

The one-dimensional or at least the quasi-one-dimensional arrangement of nanoparticles needs the help of appropriate templates or of sophisticated techniques, since nature usually does not tend to organize in one dimension for energetic reasons.

One of these techniques consists of cutting an ordered monolayer of nanoparticles into stripes. Indeed this approach works in principal, but not for generating cluster wires routinely. As is shown in Fig. 15, islands of self-assembled monolayers of $\text{Au}_{55}(\text{PPh}_3)_{12}\text{Cl}_6$, swimming on the water surface, are sectioned into narrow stripes of 3–4 cluster rows when transferred onto a substrate under very distinct conditions.²⁹

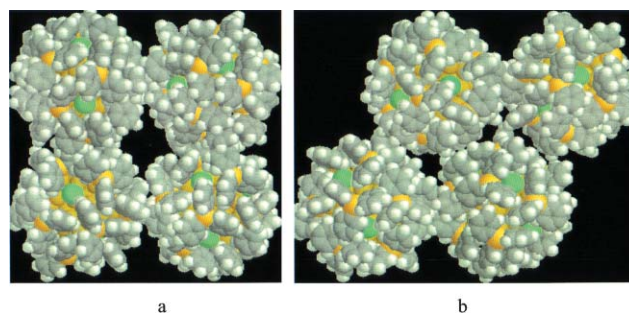


Fig. 13 Space-filling models of square (a) and hexagonally (b) oriented $\text{Au}_{55}(\text{PPh}_3)_{12}\text{Cl}_6$ clusters as observed in monolayers.

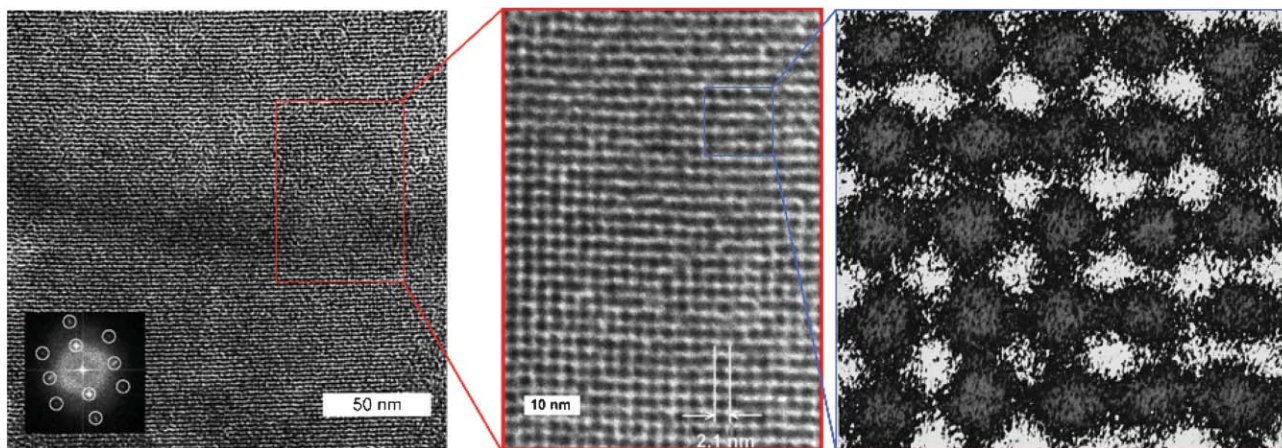


Fig. 14 TEM images of a $\text{Au}_{55}(\text{PPh}_3)_{12}\text{Cl}_6$ monolayer with increasing magnification. Insert: electron diffraction image indicating square ordering.

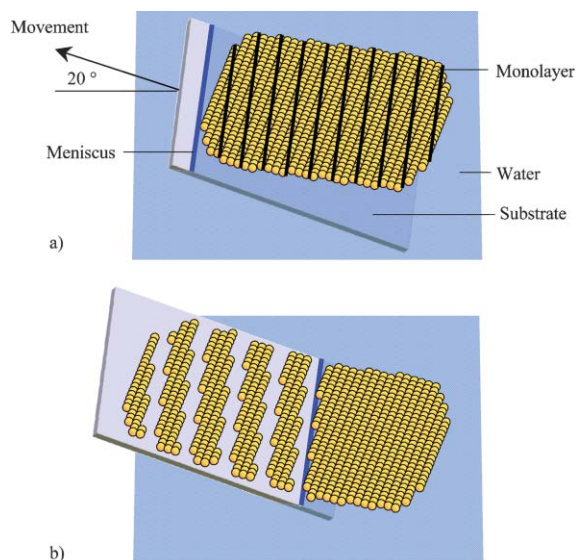


Fig. 15 Formation of stripes of $\text{Au}_{55}(\text{PPh}_3)_{12}\text{Cl}_6$ clusters by sectioning a swimming, ordered island due to an oscillating meniscus at the water–air phase boundary.

If a substrate is put underneath the island and is then withdrawn with an experimentally determined speed and an as-determined angle, the oscillating meniscus at the water–air phase boundary sections the monolayer. Fig. 16 shows a TEM image of an as-prepared assembly of such quasi-one-dimensional cluster arrangements. The difficulty to reproduce identical results makes this approach not very much suited for electrical measurements or other applications.

Polymers may serve as templates if there is a sufficient attraction between the ligand molecules and the polymer. PPE turned out to act in that way, however the results are also not so much convincing with respect to reproducibility (Fig. 17).³⁰

PVP is another polymer that can chemisorb $\text{Au}_{55}(\text{PPh}_3)_{12}\text{Cl}_6$ clusters *via* the phenyl groups in an impressive way as can be seen from Fig. 18.³¹

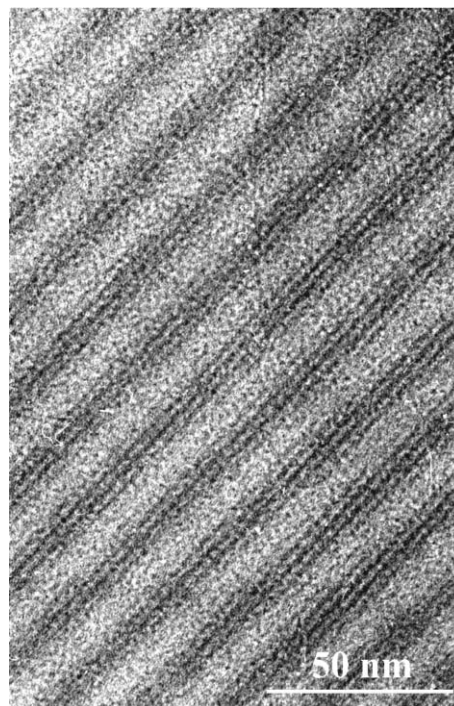


Fig. 16 TEM image of cluster stripes, each consisting of 3–4 one-dimensional rows.

The pattern of cluster-coated polymer molecules indicates that the nanoparticles partially act as linking knots between polymer chains and so generate a stable network.

Finally, there is a real chance to generate perfect one-dimensional arrangements of Au_{55} particles and, even more, to create artificial patterns of quantum dots, in principle of any construction.

A metallized AFM tip is used to oxidize the terminal CH_3 groups of a self-assembled monolayer of C_{18} -thiols by electrical pulses to give COOH functions. These can chemically be transformed in several steps to SH -functionalized patterns which then are easily decorated by

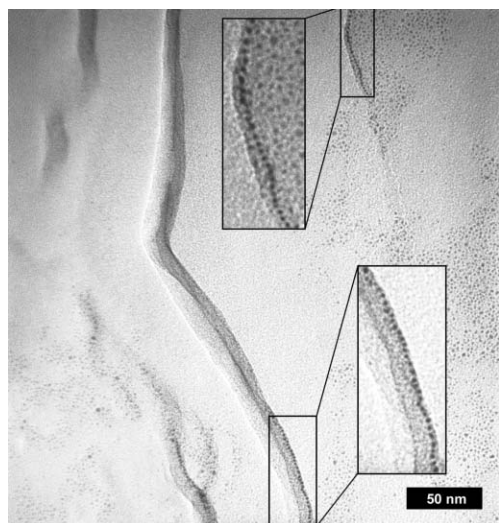


Fig. 17 TEM image of one-dimensional $\text{Au}_{55}(\text{PPh}_3)_{12}\text{Cl}_6$ on filaments of PPE.

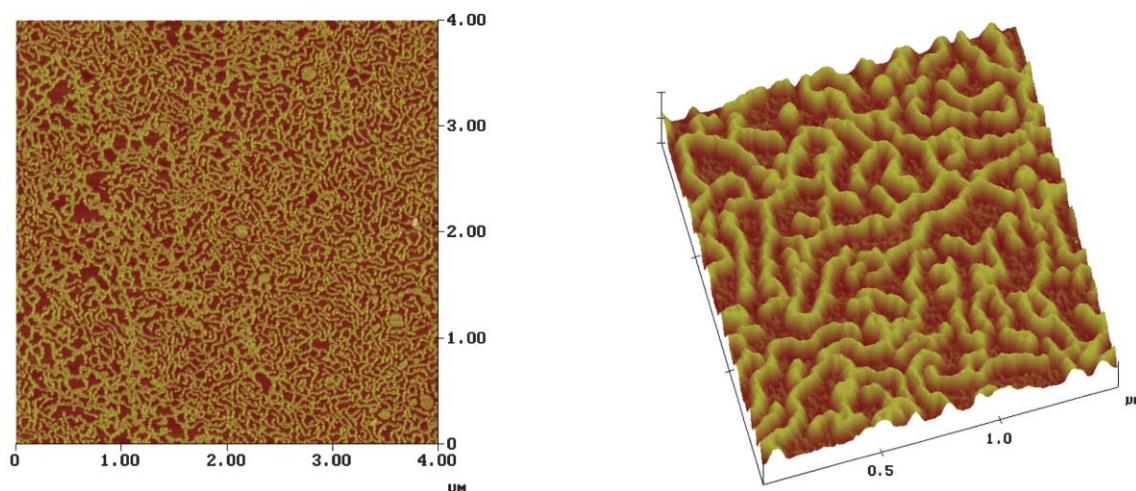


Fig. 18 AFM images of networks of PVP fibers, decorated with $\text{Au}_{55}(\text{PPh}_3)_{12}\text{Cl}_6$ clusters. The magnified cutout indicates numerous linkages, probably caused by the multifunctional clusters.

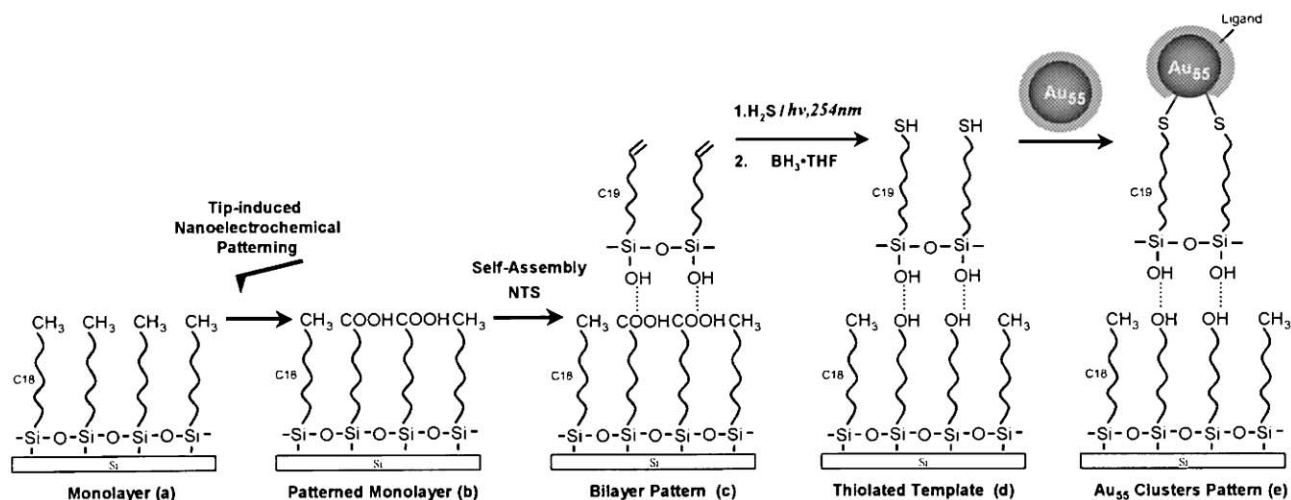


Fig. 19 Steps to generate cluster decorated surfaces.

Au_{55} clusters, simply by dipping into a cluster solution.³² Fig. 19 elucidates the various steps, whereas Figs. 20–22 show AFM images of some results.

Fig. 20a shows some chemically prepared SH-functionalized lines with the corresponding height profiles. In Fig. 20b the clusters are added and, as can be seen from the profile, the increase of height corresponds perfectly with the cluster diameters corresponding to Fig. 19. However, from high resolution AFM images it can be followed that the lines consist of two parallel cluster rows. Dots of clusters in a regular order are shown in Fig. 21. Again one registers that not one, but 2–3 particles have been deposited at one place. This is simply due to too large SH-functionalized areas as a consequence of having used too broad AFM tips. However, use of ideal tips indeed allows drawings of perfect one-dimensional lines and dots as is shown in Fig. 22.

Strictly one-dimensional wires, interrupted by deposition of 1 or 2 single clusters can be seen, as was programmed.

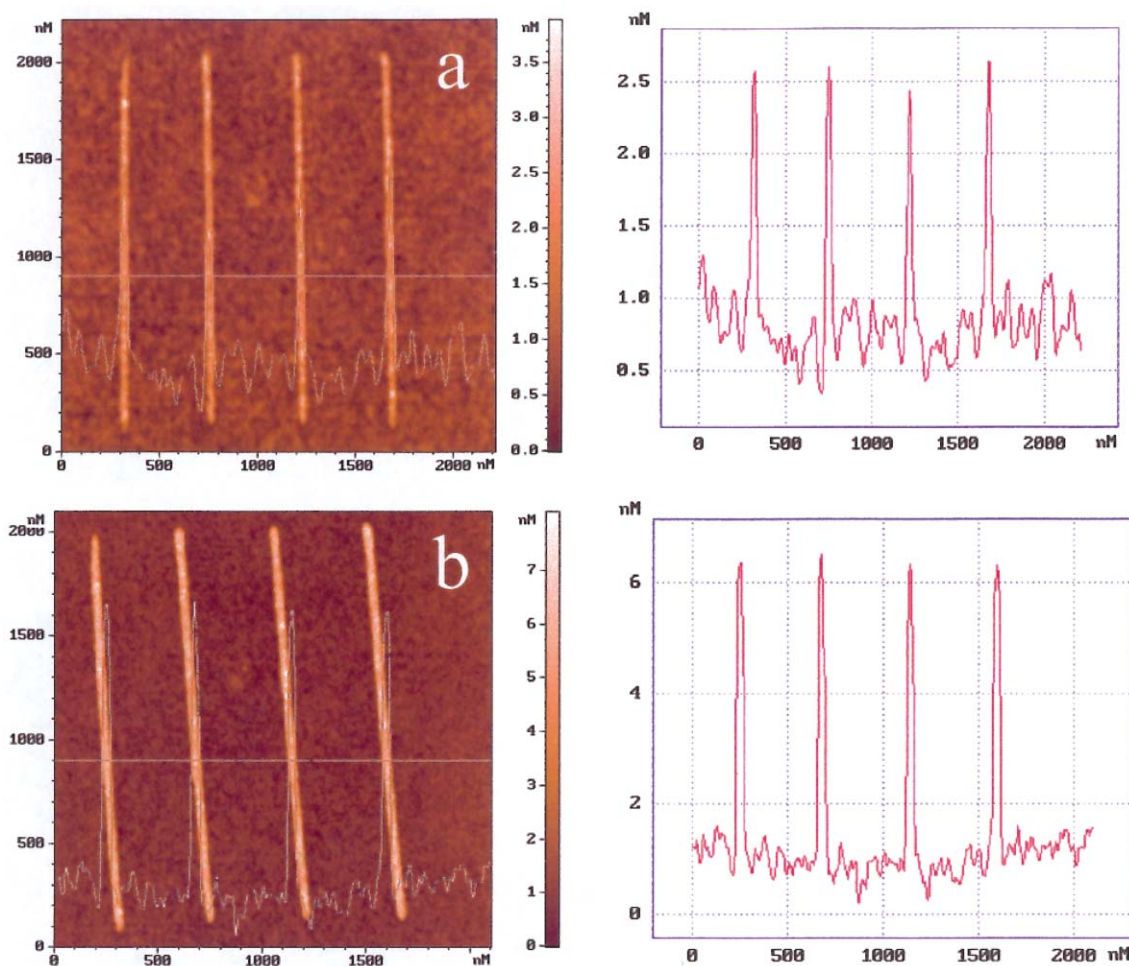


Fig. 20 Thiol-functionalized lines (a) without and (b) with clusters on top. The cross sections prove the correct heights. Magnified images show the stripes consisting of two rows of clusters.

This method will be further developed since it offers presently the most promising route to artificial structures of these single electron switches.

Electrical measurements of real 1D wires of Au₅₅ have not yet been performed, except one example using a very short “nanowire” consisting of about 6–8 particles.³³

Fig. 23 shows an SEM image of clusters arranged between two tungsten tips at a distance of *ca.* 20 nm. The positioning of the clusters succeeded by dipping the electrodes (on SiO₂) into a cluster solution with a voltage applied between the tips to electrophoretically transport the clusters and to deposit them between the electrodes. The *I(U)* characteristic of such an arrangement is also shown in Fig. 23. It exhibits a well expressed Coulomb blockade indicating a pronounced single-electron charging effect as observed for individual clusters.

Another approach for the template-mediated 1D assembly of nanoparticles is the use of DNA as an organizing molecule. Alivisatos and coworkers³⁴ showed that a discrete number of water-soluble Au₅₅ clusters with one *N*-propylmalinide ligand per cluster can couple selectively to a sulfonyl group incorporated into the single stranded DNA. Oligonucleotides, modified at either the 3' or 5' terminus with a free sulfonyl

group, were coupled with an excess of the nanoparticles. After combining with suitable oligonucleotide templates, parallel (head-to-tail) and antiparallel dimers (head-to-head) could be obtained (Fig. 24). The linear alignment of the clusters, the centre-to-centre distance which ranges from 2 to 6 nm, respectively, was illustrated by means of TEM images (Fig. 25).

Another approach for the synthesis of string-of-pearl-like alignments of Au nanoparticles along DNA strands has been reported recently.³⁶ In the first step *cis*-[Pt(NH₃)₂Cl₂] (*cis*-Pt) is intercalated into DNA double strands. This platinum complex has a high affinity to nitrogen donor sites in nucleotides and therefore binds with high selectivity in neighboring guanine–guanine nucleobases. This process is well established in medicine, where *cis*-Pt has been applied as an anti-cancer drug for more than 30 years. In its intra-strand position Pt²⁺ is now accessible for ligand exchange. Therefore, in a second step, the coupling of the nanoparticles stabilized by cysteamine can selectively bind to Pt²⁺ by exchange of the NH₃ ligands for the H₂N-termini of the ligand shell (Figs. 26 and 27).

However, all these approaches failed up to now to fabricate almost defect-free 1D arrays large enough for electrical measurements. Especially in 1D assemblies, packing defects

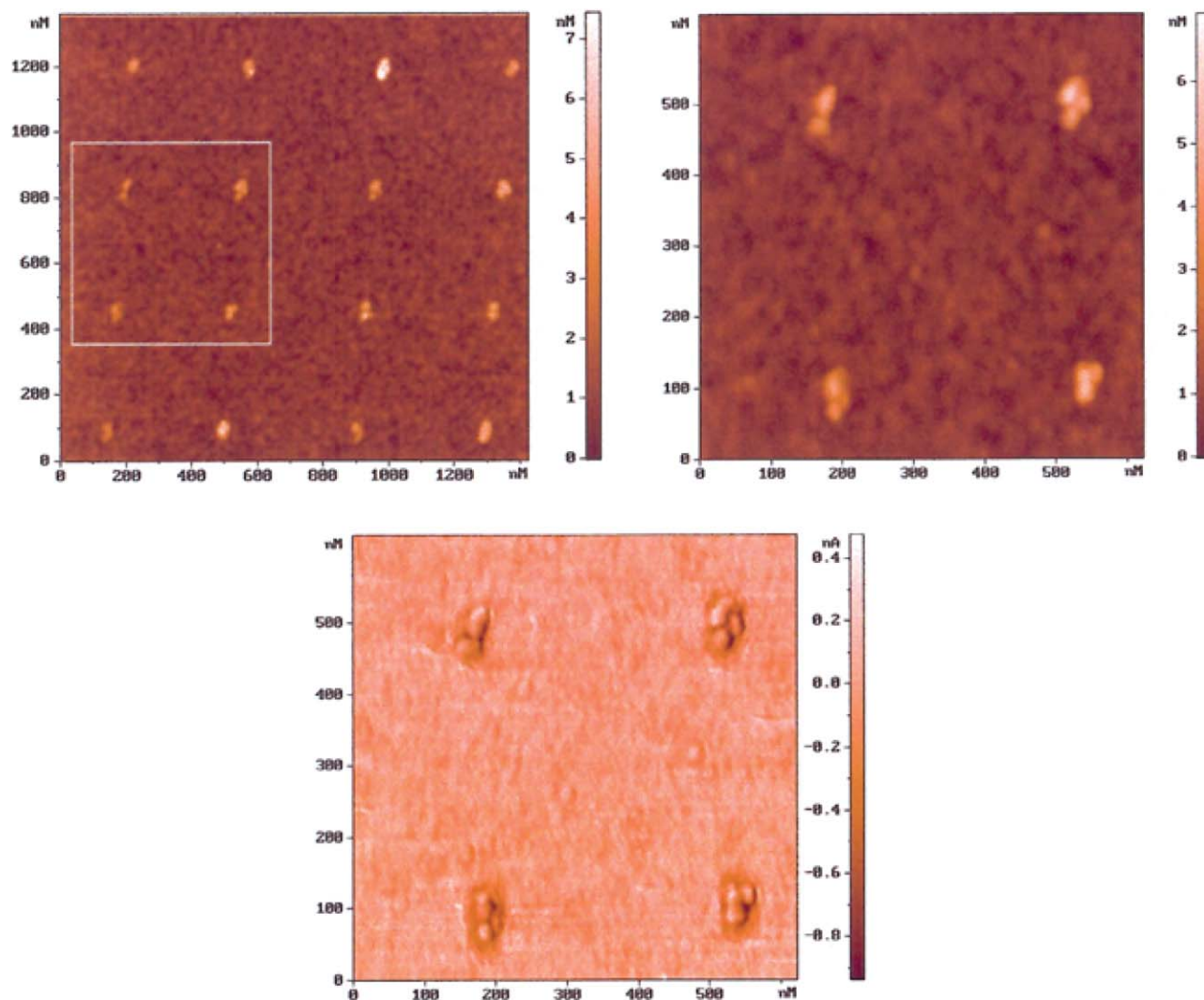


Fig. 21 Dots of $\text{Au}_{55}(\text{PPh}_3)_{12-x}\text{Cl}_6$ clusters consisting of 2–3 clusters each.

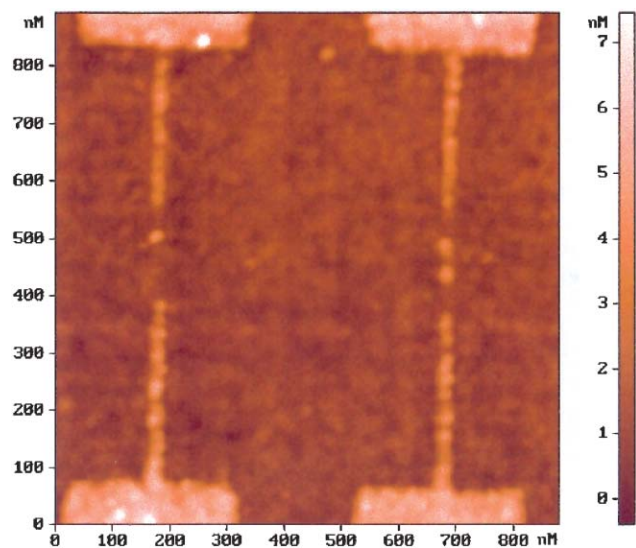
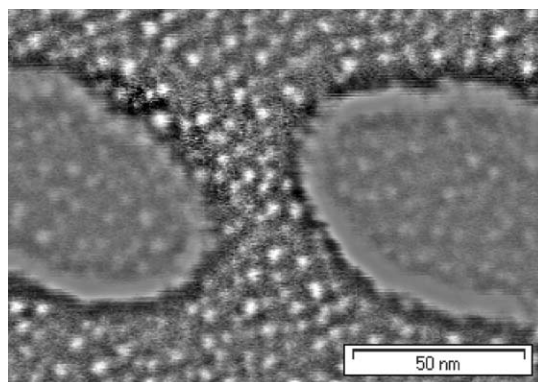


Fig. 22 Perfect one-dimensional rows of clusters, intentionally interrupted and so showing individual clusters in between.

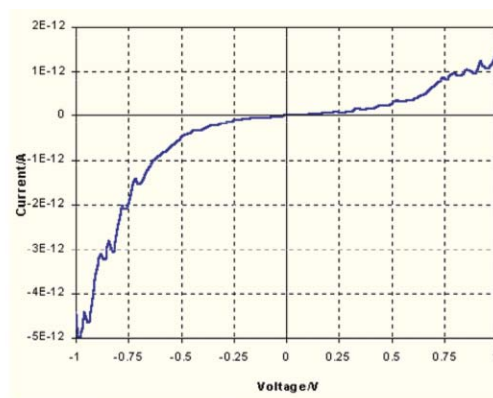
and size distribution play a crucial role with respect to reproducibility.

Conclusion

The report demonstrates that the synthesis and the organization of gold nanoparticles in 1–3 dimensions lead to unique electrical properties, caused by Coulomb charging and molecularly supported electron transfer which in principle fulfil the requirements of applicability in future microelectronics. Of course, the present day techniques which are developed on the laboratory level, are far from being satisfying for any technological process. Nevertheless, scalability and parallelization turn out to be the striking features of this approach. Besides this optimistic estimation, one has to keep in mind that the complex interplay of particle size and size distribution, of constitution, symmetry and of conformation of the ligand molecules, of the state of charge of the particles, and of the embedding media and dielectric environment is not far enough understood. Therefore, the electrical properties need to



a



b

Fig. 23 SEM image of two tungsten electrodes on SiO₂ surface with 6–8 clusters in between (a). $I(U)$ curve indicating a well expressed Coulomb blockade between *ca.* -0.3 and $+0.3$ V.

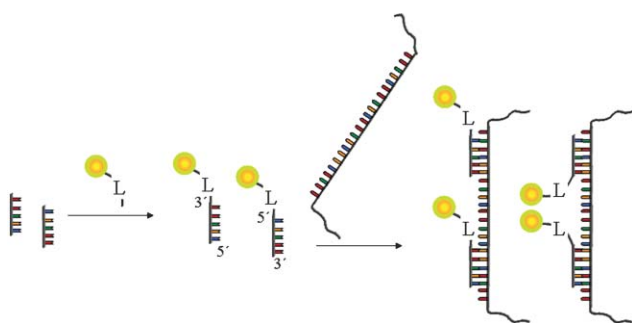


Fig. 24 Nanocrystal assembly based on Watson–Crick base-pairing interactions. Attachment of the organic nanoparticle to either the 3' or 5' terminus of the oligonucleotide “codon” by the linker L permits the preparation of head-to-head dimers or head-to-tail dimers.

be studied further to prove the reliability of the design strategies as described in this article for technological applications. With respect to circuit design, precise control over size and topology is needed. But, even the best approaches will not solve the problems of inherent defects due to orientational disorder, isotope effects, *etc.* Nevertheless, it is evident for any kind of chemical approach that falling back onto the present-day paradigm of information storage and exchange in logic elements or memory devices will require defect tolerant computer architectures with suitable, intelligent software.³⁷ Solving these problems will be the great challenges in interdisciplinary research on chemical nanostructures.

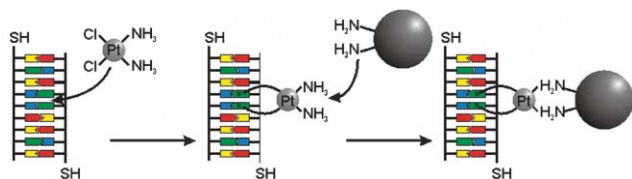


Fig. 26 Scheme for the organization of Au nanoparticles along DNA by coupling of NH₂-functionalized Au nanoparticles at *cis*-Pt-functionalized DNA *via* simple ligand replacement.

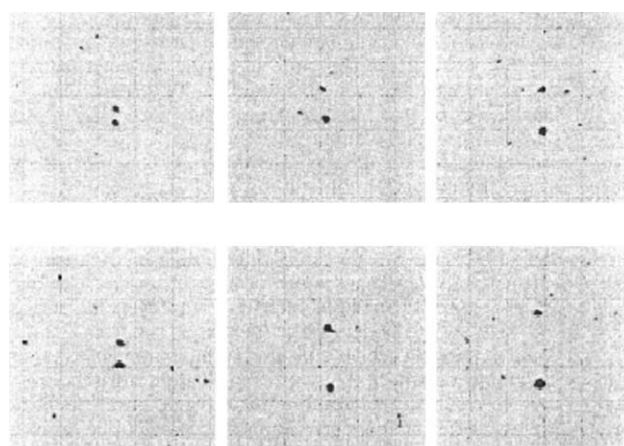


Fig. 25 TEM images of 1.4 nm Au-nucleic acid particles. (a) Head-to-head dimer sample in which a 2 : 1 ratio of 5'-HS-CAGTCAGGCAGTCAGTCA-3' strand was hybridized to the corresponding template 5'-TGACTGACTGCCTGACTGTTGACTGACTGCCTGACTG-3'. From left to right are examples of the nearest and farthest dimers (average). The centre-to-centre distances range from 2.9 ± 0.6 to 10.2 ± 0.6 nm. (b) Head-to-tail dimer sample in which a 1 : 1 ratio of 5'-HS-CTTGCACTAGTCCTTGA-3' and 5'-CAGTCAGGCAGTCAGTCA-SH-3' were hybridized to the corresponding template 5'-CTCAAGGACTAGTGCAAGTTGACTGACTGCCTGACTG-3'. From left to right are examples of the nearest, average and farthest dimers. The centre-to-centre distances in this example ranged from 2.0 ± 0.6 to 6.3 ± 0.6 nm.³⁵

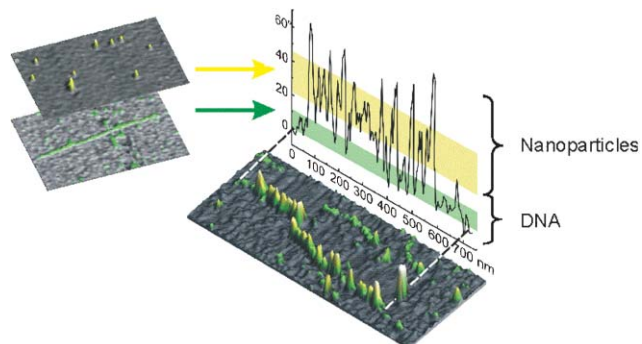


Fig. 27 AFM image (phase contrast) of DNA aligned Au nanoparticles assembled on a silicon substrate.

G. Schmid*^a and U. Simon^b

^aInstitute of Inorganic Chemistry, University of Essen, Essen, Germany.
E-mail: guenter.schmid@uni-essen.de

^bInstitute of Inorganic Chemistry, Aachen University of Technology (RWTH), Aachen, Germany

Notes and references

- 1 For a comprehensive discussion of Single Electronics and for further references see: U. Simon, in *Nanoparticles: From Theory to Application*, G. Schmid, Wiley-VCH, Weinheim, 2004.
- 2 I. Giaver and H. R. Zeller, *Phys. Rev. Lett.*, 1968, **20**, 1504.
- 3 K. K. Likharev, *IBM J. Res. Dev.*, 1998, **32**, 144.
- 4 G. Schmid and B. Corain, *Eur. J. Inorg. Chem.*, 2003, 3081.
- 5 G. Schmid, R. Pugin, T. Sawitowski, U. Simon and B. Marler, *Chem. Commun.*, 1999, 1303.
- 6 E. Emmrich, Doctoral Thesis, University of Essen, 2004.
- 7 G. Schmid, W. Meyer-Zaika, R. Pugin, T. Sawitowski, J.-P. Majoral, A.-M. Caminade and C.-O. Turrin, *Chem. Eur. J.*, 2000, **6**, 1693.
- 8 H.-G. Boyen, G. Kästle, F. Weigl, B. Koslowski, C. Dietrich, P. Ziemann, J. P. Spatz, S. Riethmüller, C. Hartmann, M. Möller, G. Schmid, M. G. Garnier and P. Oelhafen, *Science*, 2002, **297**, 1533.
- 9 G. Schmid, R. Pugin, J.-O. Malm and J.-O. Bovin, *Eur. J. Inorg. Chem.*, 1998, 813.
- 10 V. Torma, O. Vidoni, U. Simon and G. Schmid, *Eur. J. Inorg. Chem.*, 2003, 1121.
- 11 G. Schön and U. Simon, *Colloid Polym. Sci.*, 1995, **273**, 101.
- 12 G. Schön and U. Simon, *Colloid Polym. Sci.*, 1995, **273**, 202.
- 13 N. F. Mott, *Philos. Mag.*, 1969, **19**, 835.
- 14 M. P. J. van Staveren, H. B. Brom and L. J. de Jongh, *Phys. Rep.*, 1991, **208**, 1.
- 15 *Physics and Chemistry of Metal Cluster Compounds*, ed. L. J. de Jongh, Kluwer Academic Publishers, Dordrecht, 1994.
- 16 J. C. Dyre, *Phys. Rev. B*, 1993, **47**, 9128; J. C. Dyre, *Phys. Rev. B*, 1994, **49**, 11709.
- 17 S. Chen and R. Pei, *J. Am. Chem. Soc.*, 2001, **123**, 10607.
- 18 J. F. Hicks, D. T. Miles and R. W. Murray, *J. Am. Chem. Soc.*, 2002, **124**, 13322.
- 19 S. Chen, R. S. Ingram, M. J. Hostetler, J. J. Pietron, R. W. Murray, T. G. Schaaf, J. T. Khoury, M. M. Alvarez and R. L. Whetten, *Science*, 1998, **280**, 2098.
- 20 H. Taube, H. Myers and R. L. Rich, *J. Am. Chem. Soc.*, 1953, **75**, 4118.
- 21 H. Taube, *Science*, 1984, **226**, 1028.
- 22 W. P. Wuelfing, S. J. Green, J. J. Pietron, D. E. Cliffel and R. W. Murray, *J. Am. Chem. Soc.*, 2000, **122**, 11465.
- 23 V. Torma, G. Schmid and U. Simon, *Chem. Phys. Chem.*, 2001, **5**, 321.
- 24 O. Vidoni, S. Neumeier, N. Bardou, J.-L. Pelouard and G. Schmid, *J. Cluster Sci.*, 2003, **14**, 325.
- 25 E. Hesse and U. Simon, unpublished results.
- 26 G. Schmid and N. Beyer, *Eur. J. Inorg. Chem.*, 2000, 835.
- 27 Simulations performed by M. Bühl and F. Terstegen, Max Planck Institut für Kohlenforschung, Mülheim, Germany.
- 28 G. Schmid, M. Bäumlé and N. Beyer, *Angew. Chem.*, 2000, **112**, 187; *Angew. Chem., Int. Ed.*, 2000, **39**, 181.
- 29 O. Vidoni, T. Reuter, V. Torma, W. Meyer-Zaika and G. Schmid, *J. Mater. Chem.*, 2001, **11**, 3188.
- 30 D. Wyrwa, N. Beyer and G. Schmid, *Nano Lett.*, 2002, **2**, 419.
- 31 T. Reuter, O. Vidoni, V. Torma, G. Schmid, L. Nan, M. Oleiche, L. Chi and H. Fuchs, *Nano Lett.*, 2002, **2**, 709.
- 32 S. Liu, R. Maoz, G. Schmid and J. Sagiv, *Nano Lett.*, 2002, **2**, 1055.
- 33 Y. Liu, M. Schumann, T. Raschke, C. Radehaus and G. Schmid, *Nano Lett.*, 2001, **1**, 405.
- 34 A. P. Alivisatos, K. P. Johnsson, X. Peng, T. E. Wilson, C. J. Loweth, M. P. Bruchez, Jr. and P. G. Schultz, *Nature*, 1996, **382**, 609.
- 35 C. J. Loweth, W. B. Caldwell, X. Peng, A. P. Alivisatos and P. G. Schultz, *Angew. Chem., Int. Ed.*, 1999, **38**, 1808.
- 36 M. Noyong, K. Gloddek and U. Simon, *Mater. Res. Soc. Symp. Proc.*, 2003, **735**, 153.
- 37 J. R. Heath, P. Kuekes, G. Snider and S. Williams, *Science*, 1998, **280**, 1716.